Published in final edited form as:
Biomaterials. 2008 December ; 29(35): 4605–4615. doi:10.1016/j.biomaterials.2008.08.015.

Reduced Acute Inflammatory Responses to Microgel Conformal Coatings

Amanda W. Bridges[1,2], **Neetu Singh**[3], **Kellie L. Burns**[1], **Julia E. Babensee**[1,2], **L. Andrew Lyon**[1,3], and **Andrés J. García**[1,4*]

1*Petit Institute for Bioengineering and Bioscience, Georgia Institute of Technology, Atlanta, Georgia 30332-0363, USA*

2*Wallace H. Coulter Department of Biomedical Engineering, Georgia Institute of Technology, Atlanta, Georgia 30332-0363, USA*

3*School of Chemistry and Biochemistry, Georgia Institute of Technology, Atlanta, Georgia 30332-0363, USA*

4*Woodruff School of Mechanical Engineering, Georgia Institute of Technology, Atlanta, Georgia 30332-0363, USA*

Abstract

Implantation of synthetic materials into the body elicits inflammatory host responses that limit medical device integration and biological performance. This inflammatory cascade involves protein adsorption, leukocyte recruitment and activation, cytokine release, and fibrous encapsulation of the implant. We present a coating strategy based on thin films of poly(*N*-isopropylacrylamide) hydrogel microparticles (i.e. microgels) cross-linked with poly(ethylene glycol) diacrylate. These particles were grafted onto a clinically relevant polymeric material to generate conformal coatings that significantly reduced *in vitro* fibrinogen adsorption and primary human monocytes/macrophage adhesion and spreading. These microgel coatings also reduced leukocyte adhesion and expression of pro-inflammatory cytokines (TNF-α, IL-1β, MCP-1) in response to materials implanted acutely in the murine intraperitoneal space. These microgel coatings can be applied to biomedical implants as a protective coating to attenuate biofouling, leukocyte adhesion and activation, and adverse host responses for biomedical and biotechnological applications.

Keywords

cell adhesion; cytokine; foreign body response; hydrogel; macrophage; polyethylene terephthalate

1. Introduction

Host inflammatory responses to implanted biomaterials limit device integration and biological performance for most classes of medical devices, including chemical biosensors, leads and electrodes for monitoring and/or stimulation, drug delivery systems, and orthopaedic implants [1]. These inflammatory responses to synthetic materials involve dynamic, multi-component

*Corresponding author: Andrés J. García Petit Institute for Bioengineering and Bioscience 315 Ferst Drive 2314 IBB Atlanta, GA 30332-0363, USA Tel.: (404) 894-9384 Fax: (404) 385-1397 Email: andres.garcia@me.gatech.edu.

and inter-dependent reactions comprising biomolecule (e.g., protein) adsorption, leukocyte recruitment, adhesion and activation, cytokine expression/release, macrophage fusion into multi-nucleated foreign body giant cells, tissue remodeling and fibrous encapsulation [1,2]. The duration and intensity of these stages is dependent upon the extent of injury created at the implantation site and the biomaterial physicochemical properties [1].

Significant biomaterial-based efforts have focused on engineering implant surface coatings to attenuate host inflammatory responses to implanted devices. Strategies focusing on the presentation/delivery of anti-inflammatory and/or pro-wound healing agents, such as heparin, dexamethasone, and superoxide dismutase mimetics, have demonstrated promising reductions in inflammatory responses and fibrous encapsulation [3-5]. These approaches, however, are limited by complex delivery pharmacokinetics. For example, Reichert and colleagues demonstrated that combined release of dexamethasone and vascular endothelial growth factor reduced fibrous capsule thickness without changes in vascularization around implanted devices [5]. However, these benefits were lost at longer implantation times, possibly due to reductions in the release of bioactive agents. In addition to these bioactive approaches, non-fouling (i.e. protein adsorption-resistant) coatings, including dense polymeric films and brushes as well as hydrogels have been pursued to modulate inflammatory responses to implanted materials [6-15]. The rationale for these passive approaches is that reduction in protein adsorption will lead to reduced leukocyte adhesion and activation, thereby attenuating the extent of the foreign body reaction. Although many of these coatings exhibit reduced protein adsorption and leukocyte adhesion/activation *in vitro*, inconsistent results have been obtained regarding the ability of these materials to reduce *in vivo* acute and chronic inflammatory responses [6,11, 13,16]. Possible explanations for the mixed *in vivo* results with these coatings include insufficient non-fouling behavior, coating degradation, and inflammatory mechanism(s) independent from protein adsorption.

Micro- and nano-structured hydrogels offer distinct advantages over traditional surface modifications, including high water content, high diffusivity for solute transport within polymer network, and the ability to incorporate multiple chemical functionalities to generate complex architectures [17,18]. We recently developed a biomaterial coating strategy based on films of microgel particles of poly(*N*-isopropylacrylamide) (pNIPAm) cross-linked with short chains of non-fouling poly(ethylene glycol) (PEG) that render glass and polymeric substrates resistant to fibroblast adhesion *in vitro* [19]. The objective of the present study was to evaluate *in vitro* and *in vivo* inflammatory cell responses to these microgel films tethered onto poly (ethylene terephthalate) (PET). PET was chosen as the base material because this polymer is used in many biomedical devices, including sutures, vascular grafts, sewing cuffs for heart valves, and components for percutaneous access devices. PET elicits acute and chronic inflammatory responses characterized by leukocyte adhesion and fibrous encapsulation [20, 21]. Furthermore, PET has been used a model biomaterial for numerous basic biomaterial-host interactions. We demonstrate that these microgel conformal coatings reduce *in vitro* monocytes/macrophage adhesion and spreading as well as leukocyte recruitment, adhesion, and pro-inflammatory cytokine expression to implanted PET in an *in vivo* acute inflammation model.

2. Materials and methods

2.1. Sample preparation

Thin sheets of PET (AIN Plastics/ThyssenKrupp Materials NA, Madison Heights, MI) were cut into disks (8 mm diameter) using a sterile biopsy punch (Miltex Inc., York, PA) and rinsed briefly in 70% ethanol to remove contaminants introduced during the manufacturing process. pNIPAm microgel particles (100 mM total monomer concentration) were synthesized with 2 mol% PEG diacrylate (MW 575) by free radical precipitation polymerization [19]. Particles

were synthesized with 10 mol% acrylic acid as a co-monomer to incorporate functional groups for future modification. Particle composition was confirmed by NMR. Particle size (hydrodynamic radius) and polydispersity were 334 ± 30 nm and 1.11 + 0.03, respectively. Microgels were deposited on the surface of PET disks using a spin coating process as previously described [22]. All samples were rinsed in 70% ethanol on a rocker plate for 4 days, changing the solution daily to clean the samples and remove endotoxin contaminates. Prior to use, samples were rinsed three times in sterile phosphate buffered saline (PBS) and allowed to rehydrate for at least 1 h. Samples contained 10-fold lower levels of endotoxin than the United States Food and Drug Administration's recommended 0.5 EU/mL, as determined by the LAL chromogenic assay (Cambrex, East Rutherford, NJ).

2.2. Biomaterial surface characterization

X-ray photoelectron spectroscopy (XPS) analysis was performed on a Surface Science SSX-100 small spot ESCA Spectrometer using monochromatic Al K alpha X-rays, 800 μm spot size, 150 eV pass energy, and take-off angle of 55°. Atomic force microscopy (AFM) images were obtained in AC mode on an Asylum Research MFP-3D atomic force microscope. Spring constants were calculated using the thermal method. Imaging and analysis was performed using the Asylum Research MFP-3D software (written in the IgorPro environment, WaveMetrics, Inc., Lake Oswego, OR). An Olympus AC160 cantilever with k = 42 N/m, f_0 = 300 kHz was used for imaging.

2.3. Fibrinogen adsorption

Fibrinogen was selected as a model plasma protein to quantify protein adsorption onto biomaterial surfaces. The amount of surface-adsorbed protein was determined using a purified solution of radiolabeled fibrinogen diluted with unlabeled fibrinogen. Samples were incubated for 1 h in a mixture of ^{125}I-labeled human fibrinogen (65% purity, 95% clottable, specific activity of 0.86 μCi/μg, MP Biomedicals, Irvine, CA) and unlabeled human fibrinogen (65% purity, 95% clottable, Sigma-Aldrich, St. Louis, MO) to generate a range (2-200 μg/mL) of coating concentrations. Tri(ethylene glycol)-terminated self-assembled monolayers on gold-coated glass coverslips and unmodified glass coverslips were used as controls. Following incubation in fibrinogen solutions, samples were rinsed in PBS, incubated for 30 min in a 1% solution of heat-denatured bovine serum albumin (BSA), and rinsed in PBS to remove loosely adsorbed proteins. A Packard Cobra II gamma counter was used to measure the level of radiolabeled fibrinogen adsorbed onto the samples. After correcting for background and label dilution, the amount of protein adsorbed on each sample was calculated as the radioactive counts divided by the surface area and specific activity. Pilot experiments demonstrated that the albumin incubation and buffer rinses only displace a small amount (< 10%) of adsorbed fibrinogen from these surfaces.

2.4. Primary human monocyte isolation and culture

Peripheral human whole blood was obtained from healthy volunteer donors at the Georgia Institute of Technology Student Health Center in accordance with an approved Institute Review Board protocol (H05012). To prepare autologous human serum, blood (120 mL) was centrifuged (3000 rpm, 10 min, room temperature) to pellet red blood cells. The supernatant was collected, pushing down clots manually using a sterile pipette tip, and allowing further clotting (90 min, room temperature) with clearance by another centrifugation (3000 rpm, 15 minutes, room temperature).

Human monocytes were isolated from whole blood immediately after collection using an established method developed by Anderson's group [23,24] with slight modifications. Cell isolations were performed on blood from three separate donors for three independent experiments (unpooled samples) with equivalent results. Blood (120 mL) was collected in

heparin-coated syringes (333 U/mL blood, Baxter Healthcare, Deerfield, IL). The heparinized blood was transferred to polystyrene bottles (Corning, Corning, NY), diluted 1:1 with sterile PBS without calcium/magnesium, and gently swirled to mix. Peripheral blood mononuclear cells were separated using lymphocyte separation medium (Cellgro MediaTech, Herndon, VA) by differential gradient centrifugation (400*g*, 30 min at room temperature in a Thermo Fisher centrifuge, model # 5682, rotor IEC 216). The mononuclear cell layer was collected and erythrocytes lysed (155 mM ammonium chloride, 10 mM potassium bicarbonate and 0.1 mM EDTA) and washed twice with sterile PBS to remove the lysis buffer. This isolation procedure yielded > 95% viable cells as determined by Trypan blue exclusion. Flow cytometric analyses indicated 50 ± 5% monocytes (CD14+) and 46 ± 3% lymphocytes (CD14-). These yields for cell viability and monocyte fractions are consistent with previous reports [23,25].

Cells were resuspended at a concentration of 5×10^6 cells/mL in culture media (RPMI-1640 containing 25 mM HEPES, 2 mM L-glutamine [Invitrogen], 100 U/mL penicillin/streptomycin [Cellgro] and 25% filter-sterilized autologous human serum), plated in a volume of 10 mL onto 100-mm Primaria™ culture plates, and incubated at 37 °C and 5% CO_2. After 2 h, non-adherent cells were removed by rinsing three times with warm media. Cells were cultured for 10 days prior to plating onto experimental/control surfaces based on previous results showing that this time period provides for sufficient macrophage maturation [24]. Media changes occurred on days 3 and 6 of culture with media containing heat-inactivated autologous serum (56 °C, 1 h) used on day 6. By day 10 in culture, this procedure yielded 61 ± 18% macrophages (CD64+) and 29 ± 18% lymphocytes. The purity of macrophages increases with time in culture as non-adherent lymphocytes are washed away. We note that there is evidence that lymphocytes modulate and support monocyte differentiation as well as monocyte activities on biomaterials [26], suggesting that it is relevant to include this lymphocyte population in culture.

2.5. In vitro murine and human macrophage adhesion

Murine IC-21 macrophages (TIB-186, ATCC, Manassas, VA) were plated at a density of 67,000 cells/cm^2 on unmodified PET controls and microgel-coated samples. IC-21 cells were maintained in RPMI-1640 containing 25 mM HEPES, 2 mM L-glutamine, 100 U/mL penicillin/streptomycin and 10% fetal bovine serum at 37 °C and 5% CO_2. Human monocytes were plated at 50,000 cells/cm^2 on microgel-coated PET or unmodified PET controls and maintained in culture media supplemented with 25% autologous human serum at 37 °C and 5% CO_2. Following 48 h of culture, biomaterial samples were rinsed three times with sterile PBS to remove loosely adherent cells. Remaining adherent cells were stained with calcein-AM (live cells) and ethidium homodimer-1 (dead cells) (Invitrogen) and imaged using a Nikon E-400 microscope equipped with epifluorescence optics and image analysis. Five representative fields per sample (4-5 independent samples per condition) were acquired (10X Plan Fluor Nikon objective, 0.30 NA), and image analysis software (ImagePro, Media Cybernetics, Silver Spring, MD) with in-house macros was used to count adherent cells and quantify cell spreading.

2.6. Murine intraperitoneal implantation

An established intraperitoneal implantation model was used to assess acute inflammatory responses [20,27]. Animal procedures were conducted in accordance with an IACUC-approved protocol. Male 10-14 wk old C57BL/6 mice (Charles River Laboratories, Wilmington, MA) were anesthetized by isofluorane. Following a midline incision into the peritoneal cavity, sterile samples (two disks per mouse) were implanted for 48 h. Sham surgeries were performed on additional mice to be used as controls. Prior to explantation, the IP cavity was injected with 3 mL of sterile PBS containing sodium heparin (50 U/mL, Baxter Healthcare, Deerfield, IL) as an anticoagulant. The abdomen was then massaged briefly, the IP lavage fluid was collected using a syringe, and disks were retrieved for analysis. One disk was used for

immunofluorescence staining of adherent cells, and the second disk was used to harvest adherent cells for flow cytometric analysis of intracellular cytokine levels. Animals were sacrificed using a CO_2 chamber.

2.7. Immunofluorescence staining of adherent cells

Following careful explantation from the intraperitoneal cavity, biomaterial disks were stored briefly in PBS until completion of the retrieval surgery. Samples were then rinsed three times in PBS and fixed with 10% neutral buffered formalin. Adherent cells were permeabilized using 0.1% Triton-X 100 in PBS. Fetal bovine serum (5%) in PBS was used to block nonspecific protein binding. Explants were then incubated at room temperature with a primary monoclonal antibody against the macrophage marker CD68 at a 1:200 dilution (clone KP1, Abcam, Cambridge, MA). After rinsing to remove excess antibody, explants were incubated in AlexaFluor 488-conjugated goat anti-mouse IgG antibody (1:200 dilution) and counterstained with rhodamine-phalloidin (1:100 dilution) and Hoechst (1:10,000 dilution) to stain actin filaments and nuclei, respectively. Isotype control antibodies and additional staining controls demonstrated specific staining of target epitopes with minimal background. Antibodies were diluted in a solution of 1% heat-denatured BSA in PBS, and all reagents were used at 4 °C. Samples were then rinsed five times in PBS and once in deionized H_2O, mounted on glass slides with coverslips, and stored in the dark at 4 °C until imaged. Eight fields per sample were acquired (20X Plan Fluor Nikon objective, 0.45 NA), and ImagePro software (Media Cybernetics, Silver Spring, MD) with custom-designed macros was used to count the adherent cells. Results shown represent 5 or more animals per treatment group from a single implantation experiment.

2.8. Intracellular cytokine staining and flow cytometric analysis

The second disk explanted from the intraperitoneal cavity was used for measurements of cytokine expression in implant-associated cells via flow cytometry. Explanted samples were rinsed briefly in PBS and quickly transferred to a 24-well plate, and lavage samples were centrifuged to pellet cells. Cytokine staining was performed using fluorophore-labeled antibodies according to the manufacturer's protocol (eBioscience, San Diego, CA). Briefly, 1.0 mL of warm brefeldin A solution (3 μg/mL) in serum-containing media was added to each sample (disk or lavage fluid) to inhibit protein secretion into the media, and cells were incubated for 4 h at 37 °C to allow for cytokine accumulation within the cells.

Pilot experiments with different dissociation conditions were performed to identify protocols to efficiently isolate implant-associated cells with minimal cellular debris and appropriate staining and instrument settings for flow cytometry analysis. For cell harvest, samples were rinsed three times in cold PBS without calcium/magnesium. Disk-adherent cells were removed using warm trypsin (0.05% containing 0.53 mM EDTA), transferred to microcentrifuge tubes, and centrifuged at 300*g*. The resultant cell pellet was resuspended in 1.0 mL of 10% neutral buffered formalin, and tubes were shaken at low speed on a vortexer for 10 min. A series of rinse-and-centrifuge cycles were used to remove excess fixative, and cell pellets were resuspended in a combined permeabilization/blocking buffer and replaced on the vortexer for 20 min. Fluorophore-conjugated antibodies (APC-conjugated anti-mouse TNF-α [clone MP6-XT22], FITC-labeled anti-mouse IL-1β polyclonal antibody, PE anti-mouse MCP-1 [clone 2H5], FITC-labeled anti-mouse IL-10 polyclonal antibody, eBioscience) were added to the microcentrifuge tubes at the manufacturer's recommended dilutions and shaken in the dark for 1 h. A subset of samples were stained using macrophage- and neutrophil-specific markers (PE-conjugated anti-mouse F4/80 [clone BM8] and APC-labeled anti-mouse Gr1 [clone RB6-8C5] from eBioscience and Miltenyi Biotec [Auburn, CA]) to label and identify the cell populations of interest. Cells were then subjected to another series of rinse-and-centrifuge cycles to remove excess antibody and resuspended in PBS. A Becton Dickinson BD LSR digital flow cytometer

was used to measure the fluorescently-labeled intracellular cytokines (counting 10,000 events per sample), and FlowJo software v7.2 (Tree Star Inc., Ashland, OR) was used to analyze the data. Results shown represent 4-8 animals per treatment group from a single implantation experiment.

2.9. Statistical analysis

Data are presented as mean ± standard error. Statistical analysis was performed by ANOVA using Systat 11.0 (Systat Software Inc., San Jose, CA). Flow cytometry histograms were compared using the Kruskal-Wallis non-parametric test. Pair-wise comparisons were performed using Tukey post-hoc tests with a 95% confidence level considered significant.

3. Results

3.1. Deposition of microgel particles as conformal coatings

PET substrates (Fig. 1a) were functionalized with p(NIPAM-*co*-AAc-*co*-PEGDA) microgel particles (Fig. 1b and c), which were covalently attached to the surface via the incorporation of an aminobenzophenone photoaffinity label followed by UV excitation to form a covalently cross-linked coating [22] (Fig. 1). Biomaterial surfaces were analyzed for both chemical composition and the uniformity of microgel deposition using XPS and AFM, respectively. XPS survey scans revealed the presence of carbon and oxygen groups on unmodified PET controls and microgel-coated surfaces (Fig. 1d and e, respectively). Nitrogen groups (400 eV binding energy) were present only on microgel-coated surfaces (Fig. 1e). With respect to elemental composition, PET substrates contained approximately 72% carbon and 25% oxygen, whereas microgel coatings contained 77% carbon, 15% oxygen, and 9% nitrogen (all 1s orbitals). Additional high resolution scans confirmed multiple carbon bonds corresponding to the chemical structures of the PET substrate and microgel coatings (Fig. 1f and g, respectively). In particular, there was an abundance of amide bonds characteristic of pNIPAm in the microgel coating. This chemical composition is consistent with the theoretical values.

AFM images were obtained and rendered in three dimensions (Fig. 2) to visualize surface topography of the biomaterials. PET displayed a generally smooth surface (< 200 nm) exhibiting scratches and surface defects (Fig. 2a), mostly likely arising from the manufacturing process. Spin coating-based deposition of the microgel particles resulted in a conformal coating on the surface with microgel particles effectively filling in scratches and covered ridges commonly present on the surface of the underlying PET substrate (Fig. 2b). The thickness of these microgel coatings is on average 160 nm (dry) and 300 nm (swollen), as determined by AFM. Comparisons between AFM analyses of substrates with incomplete and full microgel coverage indicated monolayer particle deposition, with no evidence of multilayer formation. More expansive $50 \times 50\ \mu m^2$ scans also confirmed uniform microgel coverage (results not shown). The presence of these pNIPAm-specific nitrogen groups, along with AFM image analysis, confirms that the microgel particles were successfully deposited on the surface of PET disks.

3.2. Fibrinogen adsorption studies

We next examined the ability of these microgel coatings to attenuate protein adsorption. Fibrinogen was selected as the model protein for adsorption studies as this plasma component has been extensively studied in the context of host responses to synthetic materials. In addition to playing a central role in platelet adhesion to blood-contacting materials, fibrinogen adsorption promotes *in vitro* and *in vivo* leukocyte recruitment and adhesion to biomedical materials [20,25,27]. Protein adsorption onto the surfaces was measured using ^{125}I-labeled human fibrinogen from a purified solution (Fig. 3). Microgel-coated samples adsorbed 7-fold lower levels of fibrinogen compared to unmodified PET disks. Additionally, the PEG-based

microgel coatings performed comparably to tri(ethylene glycol)-terminated self-assembled monolayers (EG_3 SAMs) on gold-coated glass substrates, which have been extensively examined as model non-fouling surfaces [28]. Moreover, we previously demonstrated that microgel coatings reduce albumin adsorption to background levels [19]. Taken together, these results demonstrate that microgelbased coatings significantly reduce protein adsorption onto the underlying biomaterial substrate.

3.3. In vitro leukocyte adhesion

We evaluated *in vitro* monocytes/macrophage adhesion to microgel-coated and unmodified PET as a model of the leukocyte recruitment/adhesion events in the acute phase of biomaterial-induced inflammation. Murine IC-21 macrophages were plated and cultured for 48 h on biomaterials, and adherent cells were imaged and scored for viability, adherent cell density, and spread area. Unmodified PET control samples supported significant levels of cell adhesion, whereas microgel coatings exhibited 40-fold lower levels of IC-21 macrophage adhesion (Figs. 4a and 4b, respectively), as quantified in Fig. 4c ($p < 1.2\times10^{-5}$). Furthermore, cells adherent to unmodified PET samples had almost double the cytoplasmic spread area of those associated with microgel-coated samples (Fig. 4d, $p < 1.2\times10^{-5}$). Calcein-AM/ethidium homodimer (Live/Dead™) staining showed > 98% viability for both surfaces.

We performed similar studies with primary human monocytes/macrophages isolated from whole blood, as these primary cells represent a more clinically relevant model [1]. After 48 h in culture with biomaterial surfaces, adherent cells were imaged and scored for viability, adherent cell density, and spreading area. In good agreement with the murine macrophage line results, unmodified PET supported high numbers of adherent primary monocytes (Fig. 5a), whereas microgel coatings (Fig. 5b) reduced primary human monocyte/macrophage adherent cell numbers by 3-fold compared to control substrates. These results are shown graphically in Fig. 5c ($p < 1.1\times10^{-4}$). In addition, cells adherent to unmodified PET control surfaces exhibited more cell extensions and had double the cytoplasmic spread area of those associated with microgel-coated samples (Fig. 5d, $p < 1.2 \times 10^{-5}$). Calcein-AM/ethidium homodimer staining showed > 95% viability for both substrates. These results demonstrate that microgel coatings significantly reduce monocyte/macrophage adhesion and spreading compared to control PET supports.

3.4. Acute inflammatory cell responses to microgel coatings

We next evaluated early cellular responses to biomaterials implanted in the intraperitoneal cavity of mice. Tang and colleagues have established this model to examine leukocyte recruitment to implanted biomaterials during the acute inflammatory process [20,27]. Unmodified and microgel-coated PET disks (2 samples per mouse) were implanted for 48 h and then explanted and analyzed to determine leukocyte recruitment and adhesion as well as pro-inflammatory cytokine expression. Mice surgically treated but not receiving any biomaterial disks were used as sham controls.

One disk explanted from each mouse was used to examine leukocyte recruitment and adhesion by cell staining and fluorescence microscopy. Following fixation and permeabilization, adherent cells were stained using an antibody against CD68 (macrophage marker), rhodamine phalloidin (actin filaments), and Hoechst (nuclei). Unmodified PET control samples displayed a dense monolayer of adherent cells (Fig. 6a). In contrast, significantly fewer cells were attached to the microgel-coated samples (Fig. 6b). Quantification of adherent cells demonstrated a 4.6-fold reduction in cell density for microgel-coated samples compared to unmodified PET ($p < 1.1\times10^{-5}$, Fig. 6e). Furthermore, higher magnification images demonstrated fewer CD68+ macrophages on microgel-coated samples (Fig. 6d) compared to unmodified PET controls (Fig. 6c). Similar results in terms of differences in adherent cell

numbers between microgel-coated and unmodified PET surfaces were observed for in a small number of samples implanted in the murine intraperitoneal space for 16 h.

We also examined the expression of inflammatory cytokines (TNF-α, IL-1β, MCP-1, and IL-10) in implant-associated cells at 48 h of implantation by flow cytometry as a measure of leukocyte activation. This cytokine profile was selected based on previous reports of acute cytokine expression around biomaterial implants [29-32]. To ensure that the flow cytometry analysis was performed on whole cells and not debris for the harvest procedure, we first stained a subset of the harvested samples for markers characteristic of the cell populations, mainly macrophages and neutrophils. Figure 7a shows a contour profile for forward scatter (FSC, proportional to particle size) vs. side scatter (SSC, proportional to antibody staining). The profile was gated for two major areas (P1, P2). The cell population in P1, which corresponds to 85-90% of the total number of events recorded, contains particles that (i) are large enough to represent whole cells (based on FSC values) and (ii) stain positive for macrophages and neutrophils. We therefore performed analyses for cytokine expression on this P1 cell population. This type of analysis is consistent with standard immunology flow cytometric analysis [33].

Figures 7b-d present histograms showing cell counts (y-axis) as a function of cytokine staining intensity (x-axis). For TNF-α, IL-1β, and MCP-1, the histograms for microgel-coated PET show a left-ward shift compared to the histograms for untreated PET. Kruskal-Wallis non-parametric tests indicated that the histograms for microgel-coated PET were statistically different from histograms for control PET ($p < 0.02$). In addition, ANOVA of the geometric means for histograms from independent samples showed that microgel-coated samples contained significantly lower levels of pro-inflammatory TNF-α, IL-1β, and MCP-1 than unmodified PET controls (Fig. 7e-g, respectively; $p < 0.003$). No significant differences were detected between groups for levels of anti-inflammatory IL-10 (results not shown). Additionally, a peritoneal lavage was performed to collect fluid in the tissue exudates proximal to the implant. No differences were detected between surface treatments for pro-inflammatory cytokine expression of cells in the exudate, and these levels of cytokine expression were similar to the sham controls. These results demonstrate that leukocyte activation was dependent on adhesion to the biomaterial implant. Furthermore, microgel coatings attenuate leukocyte activation and significantly reduce expression of pro-inflammatory cytokines compared to PET substrates.

4. Discussion

We present a coating strategy based on thin films of poly(*N*-isopropylacrylamide-*co*-acrylic acid) hydrogel microparticles cross-linked with PEG diacrylate. These microgel particles were spin-coated and covalently grafted onto PET substrates. XPS and AFM analyses demonstrated that these particles were deposited as dense conformal coatings. Attractive features of this coating technology include (i) precise control over particle synthesis in terms of composition and structure, (ii) ability to generate complex architectures and/or functionalities, including controlled drug release, and (iii) ability to generate ‘mosaic’ complex coatings containing variations in particle composition and/or spatial arrangement via modular assembly and soft lithography [18]. In addition, these particles can be deposited onto different substrates by various means, including spin coating, centrifugation, and dip-coating. We note that the amount of mass attached with just a few chemical reactions at the surface is potentially extraordinarily high, which should be beneficial for obtaining high densities of PEG and good surface coverage. Compared to many ‘grafting-to’ and surface polymerization reactions, this approach provides a more controllable route. Nevertheless, generation of dense, conformal microgel coatings requires optimization of particle deposition parameters, including covalent tethering, and may not be easily applicable to surfaces with complex geometries/topographies.

We examined *in vitro* protein adsorption onto microgel-coated and uncoated PET using radiolabeled fibrinogen as a model plasma protein. Microgel coatings significantly reduced fibrinogen adsorption compared to unmodified PET. Additionally, the PEG-based microgel coatings performed equivalently to self-assembled monolayers presenting tri(ethylene glycol). The significant reductions in adsorbed fibrinogen for microgel coatings are in good agreement with previous results for low adsorption of serum albumin to these films [19]. We attribute the reductions in protein adsorption to microgel coatings to the presentation of PEG 'loops' at the microgel surface resulting from temperature-induced deswelling of pNIPAm at physiological temperatures [19,34]. The levels of fibrinogen adsorbed onto microgel coatings (60 ng/cm^2 at 30 μg/mL coating concentration) are comparable to protein densities (40-60 ng/cm^2) adsorbed onto PEG/PEO polymers grafted onto surfaces [35,36]. However, the density of fibrinogen adsorbed onto the microgel coatings is considerably higher than protein densities (< 10 ng/cm^2) adsorbed onto dense brushes of oligo(ethylene glycol)methacrylate and poly(2-methacryloyloxyethyl phosphorylcholine) generated by surface-initiated polymerization reactions [7,37,38]. Furthermore, the fibrinogen adsorption levels for the microgel coating are also higher than fibrinogen adsorption values (< 10 ng/cm^2) reported for glow discharge plasmadeposited tetraethylene glycol dimethyl ether densely cross-linked coatings ("tetraglyme") [25,39]. The differences in protein adsorption resistance among these coating technologies probably arise from differences in the architecture/structure of the PEG chains as the chain length and grafting density strongly influence "non-fouling" behavior [7,40]. An alternative explanation for the higher values of adsorbed fibrinogen to the microgel coatings is that there are spaces between microgel particles below the resolution of the AFM rendering that provide sites for protein adsorption. This potential limitation could be addressed by using a different deposition technique or multi-layers of microgel particles. Finally, it is important to note that additional experiments with more complex protein solutions, such as plasma, are required to fully characterize the protein-adsorption resistant properties of these coatings.

Microgel-coated PET exhibited significant reductions in *in vitro* cell adhesion and spreading compared to untreated PET for both an established murine macrophage cell line and primary human monocytes/macrophages. The reduced levels of cell adhesion and spreading on microgel-coated surfaces provide indirect evidence for the lack of adsorption of cell-adhesion promoting proteins. We observed high levels of viability between surface conditions, so we do not attribute the differences in adherent cell numbers and spreading to differences in cell viability between the surfaces. These cell adhesion results are consistent with previous reports of very low *in vitro* monocytes/macrophage adhesion to PEG-functionalized materials such as tetraglyme and PEG-star coatings [11,12]. In contrast, other studies showed high monocytes/macrophage adhesion to surfaces grafted with PEO polymers or PEG-containing interpenetrating networks [9,41]; however, *in vitro* macrophage fusion into foreign body giant cells was significantly decreased on these coatings. The reason(s) for these discrepancies in monocytes/macrophage adhesion among PEG-based coatings remains poorly understood. These PEG-based coatings significantly reduce protein adsorption, albeit to different extents, and prevent adhesion of other cell types such as osteoblasts and endothelial cells. Possible explanations include (i) differences in adhesion receptor repertoire or numbers between primary monocytes/macrophages and other cell types and (ii) increased cell type-dependent degradation/modification of the underlying PEG coating.

We evaluated acute inflammatory cellular responses to microgel coatings in a murine intraperitoneal implant model. Microgel coatings significantly reduced the number of adherent leukocytes compared to uncoated PET at 48 h of implantation. Similar differences were observed in a small number of samples implanted for 16 h. These reductions in *in vivo* leukocyte adhesion for the microgel coatings are in good agreement with our *in vitro* cell adhesion findings. Furthermore, analysis of cytokine expression in adherent leukocytes demonstrated that microgel coatings reduced expression of the pro-inflammatory cytokines TNF-α, IL-1β,

and MCP-1 compared to untreated microgel coatings following 48 h implantation. This analysis is based on comparing equal numbers of cells; because microgel-coated implants contained 4.6-fold fewer cells than untreated PET implants, we expect that the total cytokine load will be significantly reduced for the microgel-coated implants. Differences in cytokine expression were only detected for adherent cells and were not evident in cells isolated from lavage fluid, suggesting that adhesion to the implant was necessary for increased cytokine expression. Taken together, these results indicate that microgel coatings reduce acute inflammatory cell adhesion and cytokine expression *in vivo*. Finally, we note that the use of flow cytometry for analysis of cytokine expression provides a sensitive and powerful "per cell" assay that allows direct comparisons between cell populations, especially when compared to population-averaged assays such as ELISA. However, the flow cytometry-based assay is limited to measuring intracellular, but not secreted, cytokines and provides relative (not absolute) measurements.

The significant reductions in leukocyte adhesion and activation (cytokine expression) for microgel-coated PET contrast with reports for *in vivo* leukocyte adhesion to PEG/PEO-coated materials [11,16,42]. For instance, Horbett and colleagues demonstrated high levels of leukocyte adhesion to tetraglyme coatings after 1-day subcutaneous implantation [11], even though they reported reduced *in vitro* adhesion of monocytes/macrophages [43]. These investigators attributed the increased levels of *in vivo* leukocyte adhesion to degradation of the tetraglyme coating and inadequate non-fouling behavior. Interestingly, *in vitro* cell adhesion studies in the presence of whole blood or 10% autologous plasma revealed increased levels of leukocyte adhesion and spreading, consistent with the *in vivo* observations. The differences in adhesive activities between various media conditions (whole blood, 10% plasma, and 10% serum) suggest that differences in protein adsorption, possibly fibrinogen, account for the observed responses. This possibility warrants further examination. Nonetheless, it is evident from the preceding discussion that there is no simple correlation among protein adsorption, *in vitro* monocyte/macrophage adhesion, and *in vivo* leukocyte adhesion for PEG-based coatings.

Several mechanisms could explain the ability of microgel coatings to significant reduce *in vivo* leukocyte adhesion and cytokine expression, especially when considering that these coatings exhibited higher levels of protein adsorption compared to tetraglyme and other PEO-based films. First, the higher levels of adsorbed proteins may be due to adsorption in spaces between microgel particles that are inaccessible to cells, resulting in dense conformal coatings with respect to the cells. Alternatively, because our assembly process deposits a high volume polymer film (swollen microgel coatings are ~ 300 nm thick, tetraglyme coatings are 100 nm [39]), it is possible that the microgel coatings undergo slower overall degradation than other coatings. Finally, an intriguing possibility is that the topography, in combination with the surface chemistry, of the microgel coating reduces leukocyte adhesion. Siedlecki et al. recently demonstrated that sub-micron surface features (pillars) reduce platelet adhesion and activation [44]. Regardless of the underlying mechanism(s) responsible for the observed acute cellular responses, additional analyses with longer implantation times to examine chronic inflammatory responses and fibrous encapsulation are required to establish the potential of this microgel technology as a coating strategy for biomedical devices.

5. Conclusion

We present a coating strategy based on thin films of poly(*N*-isopropylacrylamide-*co*-acrylic acid) hydrogel microparticles cross-linked with poly(ethylene glycol) diacrylate. Simple spin coating and cross-linking of these particles to substrates generated conformal coatings that significantly reduced fibrinogen adsorption and *in vitro* adhesion and spreading of an established macrophage cell line and primary human monocytes. More importantly, these coatings reduced leukocyte adhesion to polymer implants and attenuated the expression of pro-

inflammatory cytokines *in vivo*. These microgel coatings can be applied to biomedical implants as a protective coating to attenuate biofouling as well as leukocyte adhesion and activation in biomedical and biotechnological applications.

Acknowledgements

This work was funded by the Georgia Tech/Emory NSF ERC on the Engineering of Living Tissues (EEC-9731643) and a Johnson & Johnson/Georgia Tech Innovation Grant. A.W.B. was supported by a NSF Graduate Research Fellowship. The authors gratefully acknowledge J.M. Anderson (Case Western Reserve Univ.) and T.A. Horbett (Univ. Washington) for helpful discussions and recommendations, as well as Sucharita Shankar (Georgia Institute of Technology) for assistance with establishing the human monocytes isolation protocol. The authors also acknowledge the assistance of the staff of the Georgia Institute of Technology Student Health Center in blood drawing.

References

1. Anderson JM, Rodriguez A, Chang DT. Foreign body reaction to biomaterials. Semin Immunol 2008;20:86–100. [PubMed: 18162407]
2. Ratner BD, Bryant SJ. Biomaterials: where we have been and where we are going. AnnuRev Biomed Eng 2004;6:41–75.
3. Crossley GH, Brinker JA, Reynolds D, Spencer W, Johnson WB, Hurd H, Tonder L, Zmijewski M. Steroid elution improves the stimulation threshold in an active-fixation atrial permanent pacing lead. A randomized, controlled study. Model 4068 Investigators. Circulation 1995;92:2935–9. [PubMed: 7586262]
4. Udipi K, Ornberg RL, Thurmond KB 2nd, Settle SL, Forster D, Riley D. Modification of inflammatory response to implanted biomedical materials in vivo by surface bound superoxide dismutase mimics. J Biomed Mater Res 2000;51:549–60. [PubMed: 10880102]
5. Norton LW, Koschwanez HE, Wisniewski NA, Klitzman B, Reichert WM. Vascular endothelial growth factor and dexamethasone release from nonfouling sensor coatings affect the foreign body response. J Biomed Mater Res A 2007;81:858–69. [PubMed: 17236219]
6. Quinn CP, Pathak CP, Heller A, Hubbell JA. Photo-crosslinked copolymers of 2-hydroxyethyl methacrylate, poly(ethylene glycol) tetra-acrylate and ethylene dimethacrylate for improving biocompatibility of biosensors. Biomaterials 1995;16:389–96. [PubMed: 7662824]
7. Ma H, Wells M, Beebe TP, Chilkoti A. Surface-initiated atom transfer radical polymerization of oligo (ethylene glycol) methyl methacrylate from a mixed self-assembled monolayer on gold. Adv Funct Mater 2006;16:640–8.
8. Zhang F, Kang ET, Neoh KG, Wang P, Tan KL. Surface modification of stainless steel by grafting of poly(ethylene glycol) for reduction in protein adsorption. Biomaterials 2001;22:1541–8. [PubMed: 11374453]
9. Collier TO, Anderson JM, Brodbeck WG, Barber T, Healy KE. Inhibition of macrophage development and foreign body giant cell formation by hydrophilic interpenetrating polymer network. J Biomed Mater Res 2004;69A:644–50.
10. Lee JH, Kopeckova P, Kopecek J, Andrade JD. Surface properties of copolymers of alkyl methacrylates with methoxy (polyethylene oxide) methacrylates and their application as protein-resistant coatings. Biomaterials 1990;11:455–64. [PubMed: 2242394]
11. Shen M, Martinson L, Wagner MS, Castner DG, Ratner BD, Horbett TA. PEO-like plasma polymerized tetraglyme surface interactions with leukocytes and proteins: in vitro and in vivo studies. J Biomater Sci Polym Ed 2002;13:367–90. [PubMed: 12160299]
12. Wagner VE, Bryers JD. Monocyte/macrophage interactions with base and linear- and star-like PEG-modified PEG-poly(acrylic acid) co-polymers. J Biomed Mater Res A 2003;66:62–78. [PubMed: 12833432]
13. Hyung Park J, Bae YH. Hydrogels based on poly(ethylene oxide) and poly(tetramethylene oxide) or poly(dimethyl siloxane). III. In vivo biocompatibility and biostability. J Biomed Mater Res A 2003;64:309–19. [PubMed: 12522818]

14. Norton LW, Tegnell E, Toporek SS, Reichert WM. In vitro characterization of vascular endothelial growth factor and dexamethasone releasing hydrogels for implantable probe coatings. Biomaterials 2005;26:3285–97. [PubMed: 15603824]
15. Tan J, Brash JL. Nonfouling biomaterials based on polyethylene oxide-containing amphiphilic triblock copolymers as surface modifying additives: Adsorption of proteins from human plasma to copolymer/polyurethane blends. J Biomed Mater Res A. May 19;2008 Epub
16. Ronneberger B, Kao WJ, Anderson JM, Kissel T. In vivo biocompatibility study of ABA triblock copolymers consisting of poly(L-lactic-co-glycolic acid) A blocks attached to central poly (oxyethylene) B blocks. J Biomed Mater Res 1996;30:31–40. [PubMed: 8788103]
17. Pelton RH. Temperature-sensitive aqueous microgels. Adv Colloid Interface Sci 2000;85:1–33. [PubMed: 10696447]
18. Nayak S, Lyon LA. Soft nanotechnology with soft nanoparticles. Angew Chem Int Ed Engl 2005;44:7686–708. [PubMed: 16283684]
19. Nolan CM, Reyes CD, Debord JD, Garcia AJ, Lyon LA. Phase transition behavior, protein adsorption, and cell adhesion resistance of poly(ethylene glycol) cross-linked microgel particles. Biomacromolecules 2005;6:2032–9. [PubMed: 16004442]
20. Tang L, Eaton JW. Fibrin(ogen) mediates acute inflammatory responses to biomaterials. J Exp Med 1993;178:2147–56. [PubMed: 8245787]
21. van der Giessen WJ, Lincoff AM, Schwartz RS, van Beusekom HM, Serruys PW, Holmes DR Jr. Ellis SG, Topol EJ. Marked inflammatory sequelae to implantation of biodegradable and nonbiodegradable polymers in porcine coronary arteries. Circulation 1996;94:1690–7. [PubMed: 8840862]
22. Singh N, Bridges AW, Garcia AJ, Lyon LA. Covalent tethering of functional microgel films onto poly(ethylene terephthalate) surfaces. Biomacromolecules 2007;8:3271–5. [PubMed: 17877399]
23. McNally AK, Anderson JM. Complement C3 participation in monocyte adhesion to different surfaces. Proc Natl Acad Sci USA 1994;91:10119–23. [PubMed: 7937848]
24. McNally AK, Anderson JM. Interleukin-4 induces foreign body giant cells from human monocytes/macrophages. Differential lymphokine regulation of macrophage fusion leads to morphological variants of multinucleated giant cells. Am J Pathol 1995;147:1487–99. [PubMed: 7485411]
25. Shen M, Horbett TA. The effects of surface chemistry and adsorbed proteins on monocyte/macrophage adhesion to chemically modified polystyrene surfaces. J Biomed Mater Res 2001;57:336–45. [PubMed: 11523028]
26. Chang DT, Colton E, Anderson JM. Paracrine and juxtacrine lymphocyte enhancement of adherent macrophage and foreign body giant cell activation. J Biomed Mater Res A. Apr 24;2008 Epub
27. Hu WJ, Eaton JW, Ugarova TP, Tang L. Molecular basis of biomaterial-mediated foreign body reactions. Blood 2001;98:1231–8. [PubMed: 11493475]
28. Prime KL, Whitesides GM. Adsorption of proteins onto surfaces containing end-attached oligo (ethylene oxide): a model system using self-assembled monolayers. J Am Chem Soc 1993;115:10714–21.
29. Suska F, Esposito M, Gretzer C, Kalltorp M, Tengvall P, Thomsen P. IL-1alpha, IL-1beta and TNF-alpha secretion during in vivo/ex vivo cellular interactions with titanium and copper. Biomaterials 2003;24:461–8. [PubMed: 12423601]
30. Luttikhuizen DT, van Amerongen MJ, de Feijter PC, Petersen AH, Harmsen MC, van Luyn MJ. The correlation between difference in foreign body reaction between implant locations and cytokine and MMP expression. Biomaterials 2006;27:5763–70. [PubMed: 16934325]
31. Baldwin L, Hunt JA. The in vivo cytokine release profile following implantation. Cytokine 2008;41:217–22. [PubMed: 18221883]
32. Rodriguez A, Meyerson H, Anderson JM. Quantitative in vivo cytokine analysis at synthetic biomaterial implant sites. J Biomed Mater Res A. Apr 22;2008 Epub
33. Coligan, JE.; Bierer, B.; Margulies, DH.; Shevach, EM.; Strober, W.; Coico, R., editors. Current Protocols in Immunology. John Wiley & Sons; New York: 2007. Immunofluorescence and Cell Sorting.
34. Gan D, Lyon LA. Synthesis and protein adsorption resistance of PEG-modified poly(N-isopropylacrylamide) core/shell microgels. Macromolecules 2002;35:9634–9.

35. Jenney CR, Anderson JM. Adsorbed serum proteins responsible for surface dependent human macrophage behavior. J Biomed Mater Res 2000;49:435–47. [PubMed: 10602077]

36. Unsworth LD, Sheardown H, Brash JL. Protein resistance of surfaces prepared by sorption of end-thiolated poly(ethylene glycol) to gold: effect of surface chain density. Langmuir 2005;21:1036–41. [PubMed: 15667186]

37. Feng W, Brash JL, Zhu S. Non-biofouling materials prepared by atom transfer radical polymerization grafting of 2-methacryloloxyethyl phosphorylcholine: separate effects of graft density and chain length on protein repulsion. Biomaterials 2006;27:847–55. [PubMed: 16099496]

38. Petrie TA, Raynor JE, Reyes CD, Burns KL, Collard DM, Garcia AJ. The effect of integrin-specific bioactive coatings on tissue healing and implant osseointegration. Biomaterials 2008;29:2849–57. [PubMed: 18406458]

39. Cao L, Chang M, Lee CY, Castner DG, Sukavaneshvar S, Ratner BD, Horbett TA. Plasmadeposited tetraglyme surfaces greatly reduce total blood protein adsorption, contact activation, platelet adhesion, platelet procoagulant activity, and in vitro thrombus deposition. J Biomed Mater Res A 2007;81:827–37. [PubMed: 17236214]

40. Unsworth LD, Sheardown H, Brash JL. Protein-resistant poly(ethylene oxide)-grafted surfaces: chain density-dependent multiple mechanisms of action. Langmuir 2008;24:1924–9. [PubMed: 18217777]

41. Jenney CR, Anderson JM. Effects of surface-coupled polyethylene oxide on human macrophage adhesion and foreign body giant cell formation in vitro. J Biomed Mater Res 1999;44:206–16. [PubMed: 10397922]

42. Suggs LJ, Shive MS, Garcia CA, Anderson JM, Mikos AG. In vitro cytotoxicity and in vivo biocompatibility of poly(propylene fumarate-co-ethylene glycol) hydrogels. J Biomed Mater Res 1999;46:22–32. [PubMed: 10357132]

43. Shen M, Pan YV, Wagner MS, Hauch KD, Castner DG, Ratner BD, Horbett TA. Inhibition of monocyte adhesion and fibrinogen adsorption on glow discharge plasma deposited tetraethylene glycol dimethyl ether. J Biomater Sci Polym Ed 2001;12:961–78. [PubMed: 11787523]

44. Milner KR, Snyder AJ, Siedlecki CA. Sub-micron texturing for reducing platelet adhesion to polyurethane biomaterials. J Biomed Mater Res A 2006;76:561–70. [PubMed: 16278867]

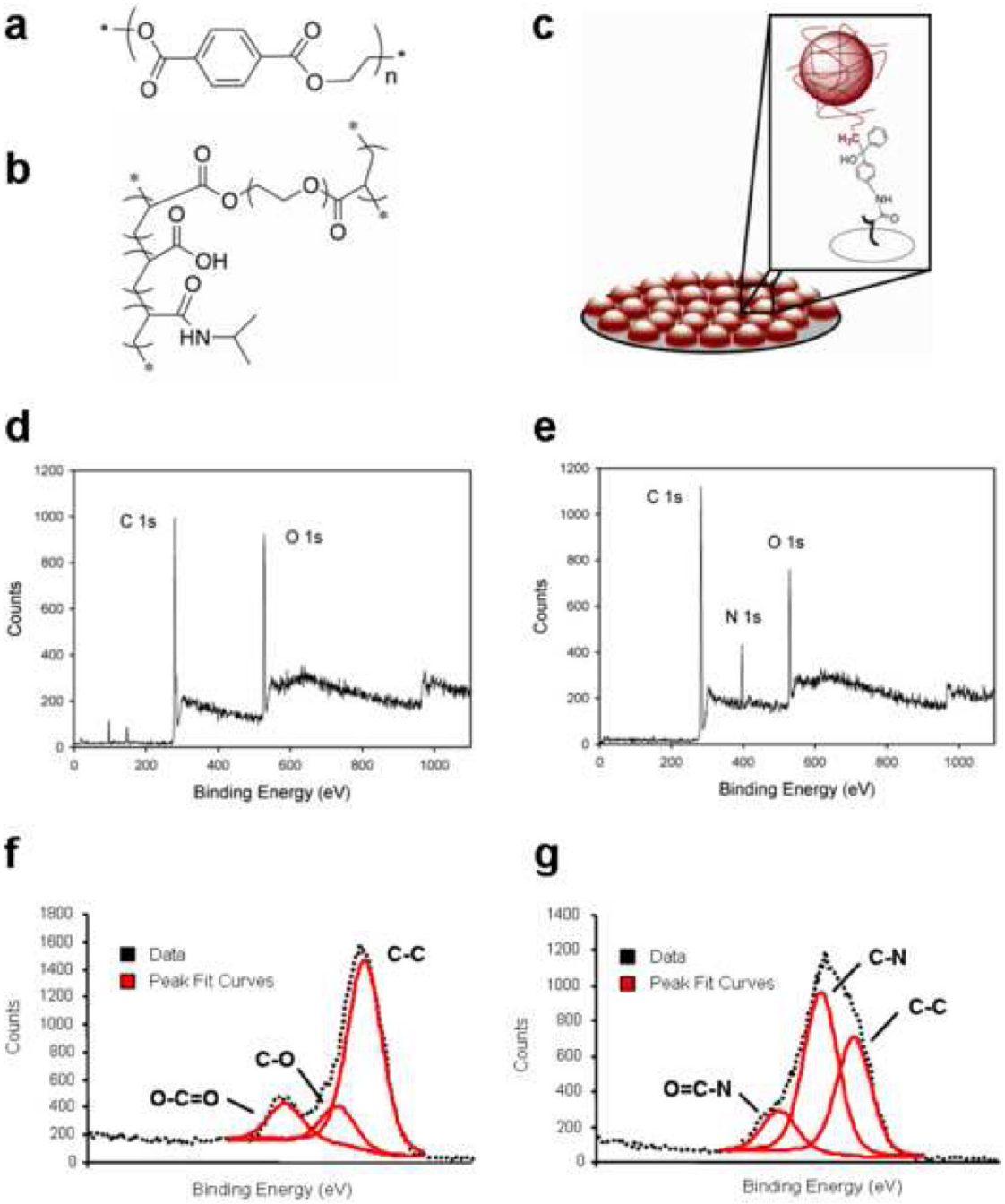

Figure 1. Surface characterization of biomaterials

Chemical structures of the unmodified PET **(a)** and p(NIPAM-*co*-AAc-*co*-PEGDA) microgel particles **(b)** are shown for reference. **(c)** Microgel particles (red spheres) are covalently attached to the surface of the underlying PET substrate (gray disk) by photo-crosslinking to create a polymeric coating. XPS analysis reveals the presence of nitrogen groups characteristic of C-N bonds on the surface of microgel-coated PET **(e)** that are absent in unmodified PET controls **(d)**. High resolution carbon 1s data was deconvoluted, and software was used to assign peak values and determine individual carbon bonds. Results are shown for unmodified PET **(f)** and microgel-coated PET **(g)**. Importantly, microgel coatings contain C-N bonds, characteristic of the amide groups in the pNIPAm particles.

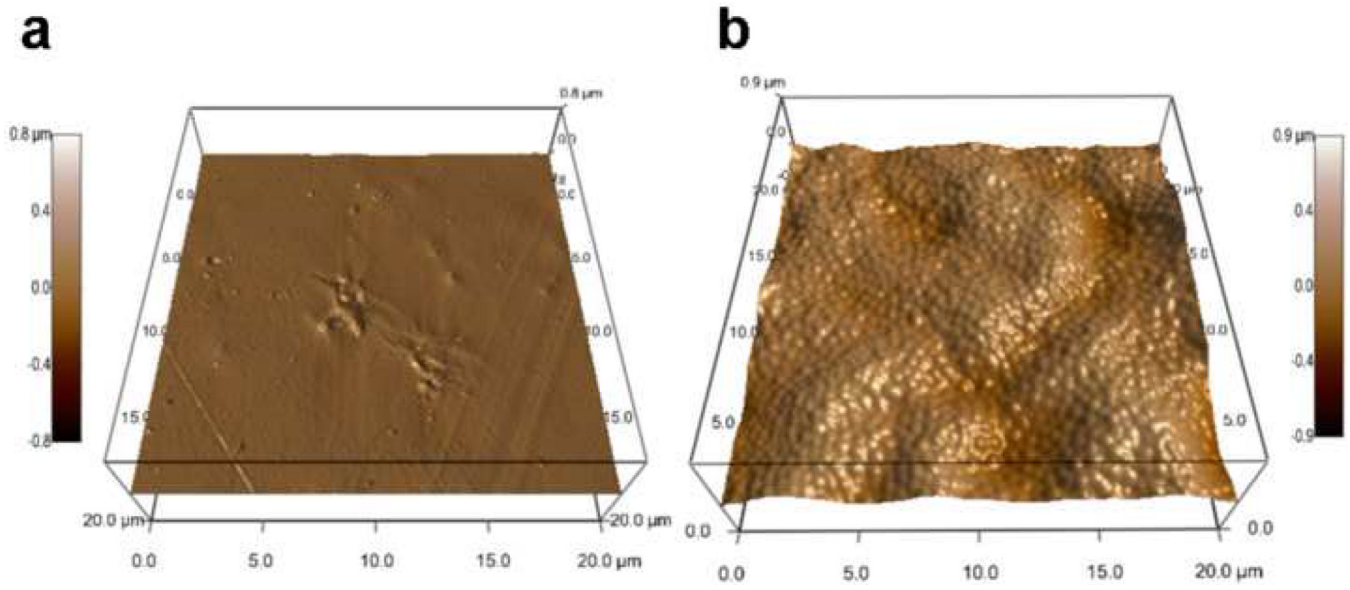

Figure 2. Topography of biomaterial surfaces

Representative 3D renderings of atomic force microscopy images demonstrate that the functionalization strategy yields a conformal coating of microgel particles **(b)** compared to unmodified PET controls **(a)**.

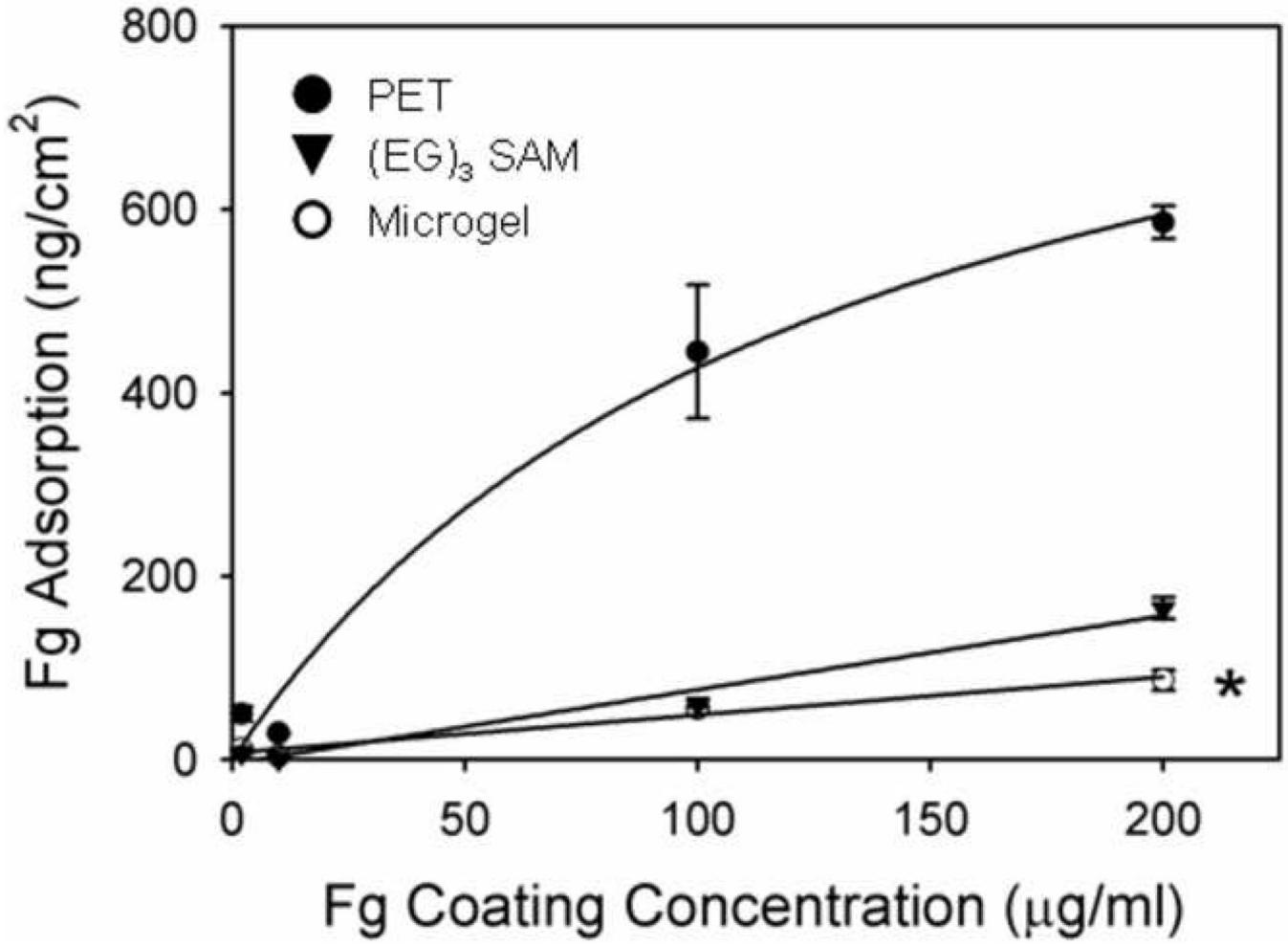

Figure 3. Protein adsorption profiles on biomaterial surfaces

Microgel-coated surfaces adsorb 7-fold lower levels of purified human fibrinogen than unmodified PET controls and also display comparable biofouling resistance to tri(ethylene glycol)-terminated self-assembled monolayers on gold, * $p < 0.001$.

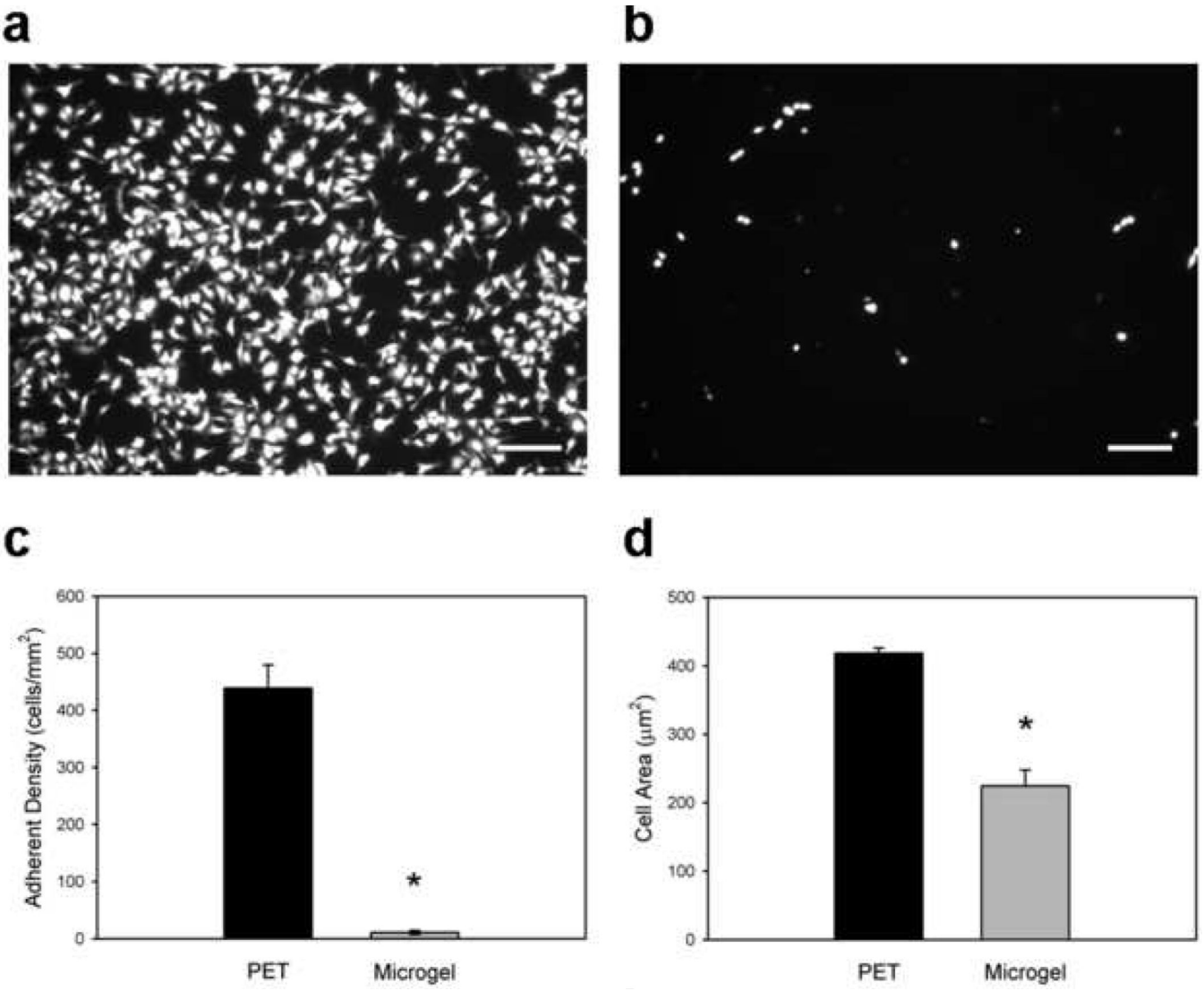

Figure 4. Murine IC-21 macrophage adhesion to biomaterial surfaces

Adherent cells were scored for viability, and cell density and area were quantified. Compared to unmodified PET substrates **(a)**, microgel coatings **(b)** reduce macrophage adhesion to biomaterial surfaces. **(c)** Unmodified PET supported 40-fold higher levels of adherent macrophages compared to microgel-coated samples, which virtually eliminated cell adhesion, * $p < 1.2\times10^{-5}$. **(d)** Adherent macrophages also exhibited more cell extensions and significantly larger surface areas on unmodified PET controls than on microgel-coated surfaces, * $p < 1.2\times10^{-5}$. Data is presented as the average value ± standard error of the mean using n = 5 samples per treatment group. Scale bar is 100 μm.

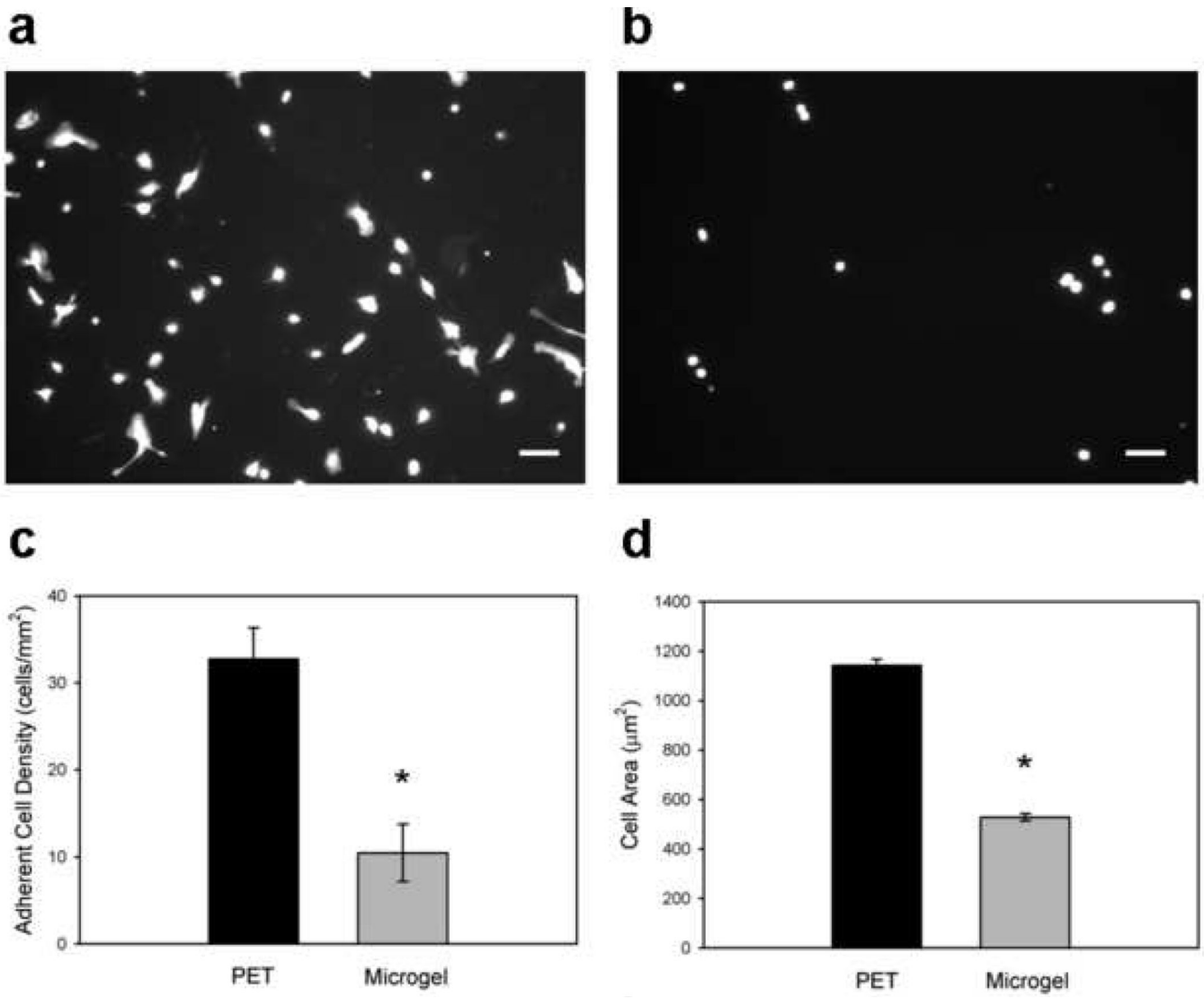

Figure 5. ***In vitro*** **human primary macrophage adhesion to biomaterial surfaces**

Adherent cells were scored for viability, and cell density and spread area were quantified. Compared to unmodified PET substrates **(a)**, microgel coatings **(b)** reduce macrophage adhesion to biomaterial surfaces. **(c)** Microgel coatings elicit a 3-fold reduction in cell adhesion compared to unmodified PET surfaces, * $p < 1.1\times10^{-4}$. **(d)** Adherent macrophages also exhibit more cell extensions and 2-fold larger surface areas on unmodified PET controls than on microgel-coated surfaces, * $p < 9.5\times10^{-7}$. Data is presented as the average value ± standard error of the mean using n = 5 samples per treatment group. Scale bar is 100 μm.

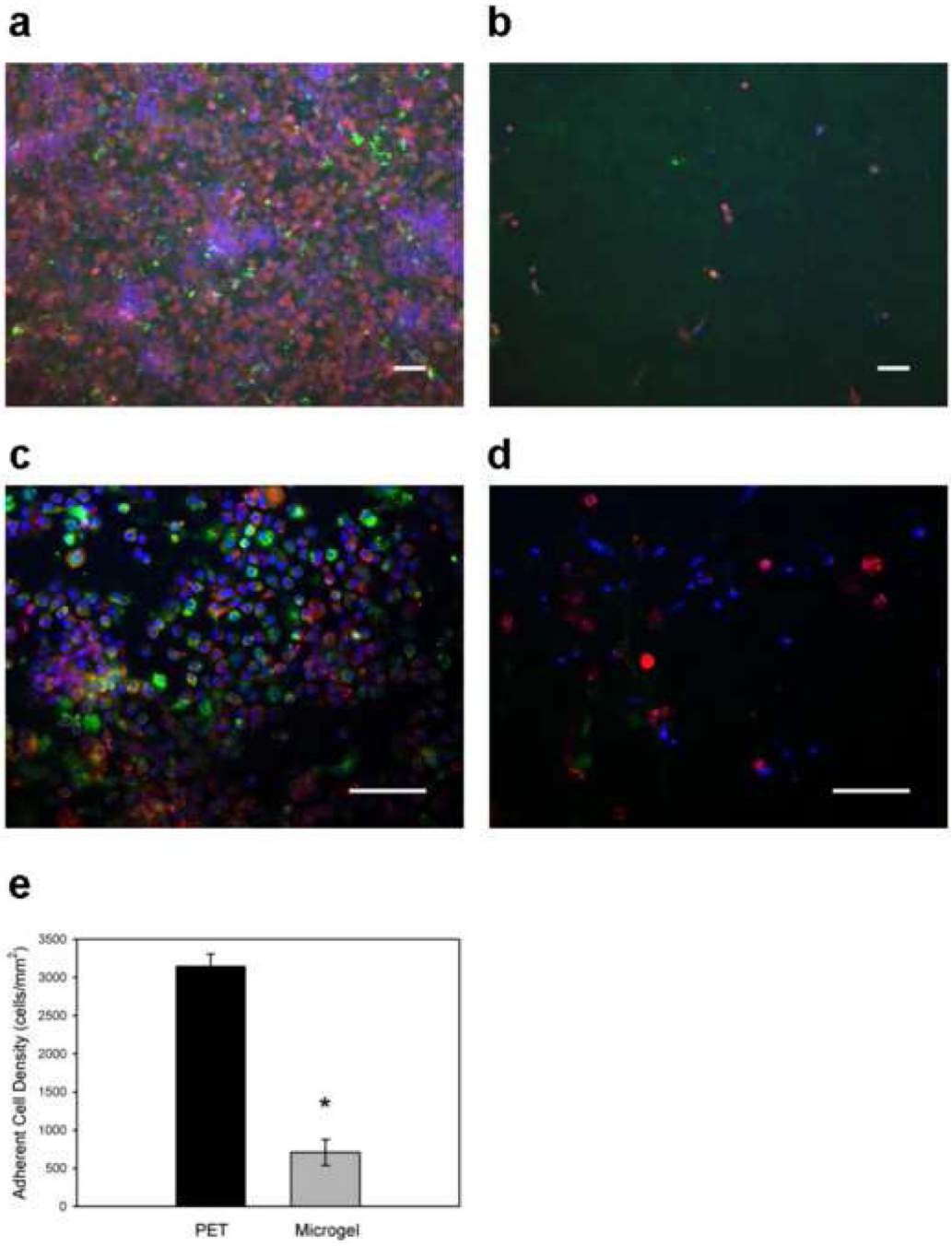

Figure 6. ***In vivo*** **leukocyte adhesion to implanted biomaterials**

Biomaterial disks were implanted in the murine peritoneal cavity for 48 h. Explants were immunostained for macrophage marker CD68 (green), actin (red), and DNA (blue). Representative images taken with 20X **(a, b)** and 40X **(c, d)** objectives are presented. In contrast to unmodified PET controls **(a)**, microgel-coated disks **(b)** effectively reduced leukocyte adhesion on these implants by a factor greater than 4-fold as quantified in **(e)**, * $p < 1.1\times10^{-5}$. In addition, fewer macrophages were observed on microgel-coated **(d)** surfaces than on unmodified PET controls **(c)**. Data is represented as the average value ± standard error of the mean using n = 5 or more samples per treatment group. Scale bar is 50 μm.

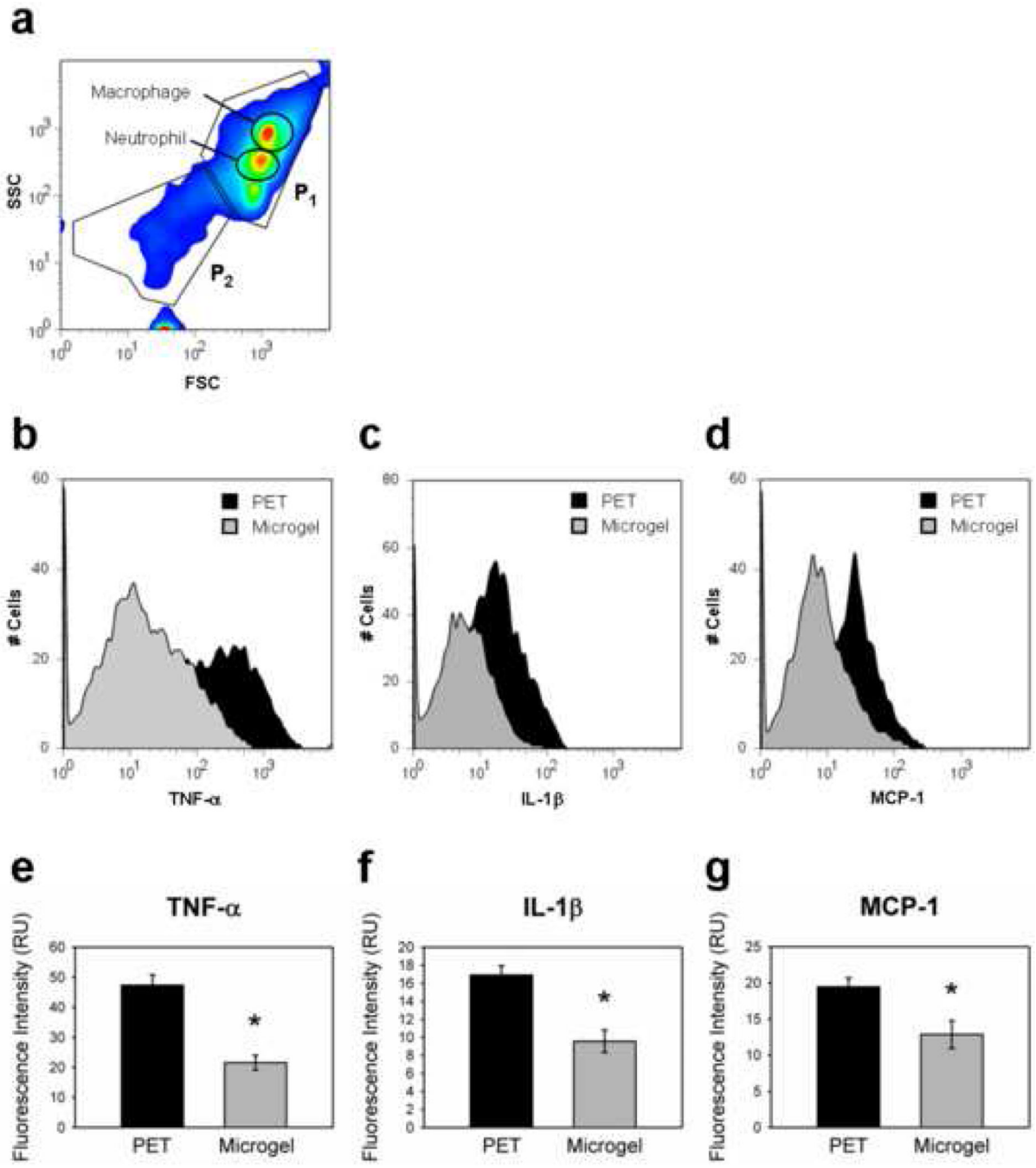

Figure 7. Quantification of *in vivo* intracellular cytokine expression by flow cytometric analysis

Disk-associated cells were harvested from implants and stained intracellularly for various cytokines, and several samples were stained for macrophage- or neutrophil-specific extracellular markers. **(a)** Two main populations of cells (P_1 and P_2) were observed on FSC vs. SSC plots. Macrophage and neutrophil populations of interest were both contained within P_1, so cytometry profiles were gated using P_1 for all subsequent data analysis. **(b, c, d)** Representative histograms show a significant population shift between unmodified PET controls and microgel-coated PET for the three cytokines examined. **(e, f, g)** Cells adherent to unmodified PET samples contained significantly higher levels of intracellular TNF-α **(e)**, IL-1β **(f)**, and MCP-1 **(g)** than microgel-coated samples, * $p < 0.003$. Data is presented as the

unbiased geometric means of the populations ± standard error of the mean using n = 4 or more samples per treatment group.